Thermophoresis of an Aerosol Sphere Parallel to One or Two Plane Walls

Huan J. Keh and Po Y. Chen
Dept. of Chemical Engineering, National Taiwan University, Taipei 106-17, Taiwan, ROC

The steady thermophoretic motion of a spherical particle in a gaseous medium located in an arbitrary position between two infinite parallel-plane walls is studied theoretically in the absence of fluid inertia and thermal convection. The Knudsen number is assumed small to describe the fluid flow by a continuum model with a temperature jump, thermal slip, and frictional slip at the particle surface. The imposed temperature gradient is constant and parallel to the two plane walls, which may be insulated or prescribed with the far-field temperature distribution. The presence of neighboring walls causes two basic effects on the particle velocity: the local temperature gradient on the particle surface is enhanced or reduced by the walls, to speed up or slow down the particle; the walls increase viscous retardation of the moving particle. A boundary collocation method is used to solve the thermal and hydrodynamic governing equations of the system. Numerical results for the thermophoretic velocity of the particle relative to that under identical conditions in an unbounded gaseous medium are presented for various relative thermal conductivity and surface properties of the particle, as well as relative separation distances between the particle and two plates. For thermophoretic motions of a spherical particle parallel to a single plate and on the central plane of a slit, the collocation results agree well with the approximate analytical solutions obtained by a method of reflections. The presence of lateral walls can reduce or enhance the particle velocity, depending on the relative thermal conductivity and surface properties of the particle, the relative particle-wall separation distances, and the thermal boundary condition at the walls. In general, the boundary effect on thermophoresis is complicated and weaker than that on sedimentation.

Introduction

Thermophoresis refers to the motion of aerosol particles in response to a temperature gradient. This phenomenon was first described in 1870 by Tyndall, who observed a dust-free zone in a dusty gas around a hot body (Waldmann and Schmitt, 1966; Bakanov, 1991). Being a mechanism for the capture of aerosol particles on cold surfaces, thermophoresis is of considerable importance in many practical applications. For example, thermophoresis can be effective in removing or collecting small particles from laminar gas streams in air-cleaning and aerosol-sampling devices (Batchelor and Shen, 1985; Sasse et al., 1994). The phenomenon has also been cited as an origin for the deposition of particulate matter on surfaces of heat exchangers, causing scale formation with the attendant reduction of the heat-transfer coefficient (Friedlander, 1977; Montassier et al., 1991). Convincing evidence has been provided that, in the modified chemical-vapor deposition process for the manufacture of high-quality optical fibers, thermophoresis is the primary mechanism responsible for the deposition of aerosol particles (soot) onto the inner walls of the containing tube (Simpkins et al., 1979; Weinberg, 1982; Morse et al., 1985). On the other hand, deposition of contaminant particles by thermophoresis on wafers in clean rooms during manufacturing steps can be a major cause of loss of product yields in the microelectronics industry (Ye et al., 1991). In the area of nuclear safety, knowledge of thermophoresis is required to calculate the deposition rates of radioactive aerosol particles released in reactor accident situations where large temperature gradients exist (Williams, 1986; Williams and Loyalka, 1991).

Correspondence concerning this article should be addressed to H. J. Keh.

The thermophoretic effect can be explained in part by appealing to the kinetic theory of gases (Kennard, 1938). The higher energy molecules in the hot region of the gas impinge on the particles with greater momenta than molecules coming from the cold region, thus leading to the migration of the particles in the direction opposite to the temperature gradient. It is convenient to express the thermophoretic velocity of an isolated particle in a constant-temperature gradient, ∇T_∞, as

$$\boldsymbol{U}_0 = -A\nabla T_\infty \tag{1}$$

where the negative sign indicates that the motion is in the direction of decreasing temperature. The thermophoretic mobility, A, depends on the magnitude of the Knudsen number, l/a, where l is the mean free path of the gas molecules and a is the radius of the particle.

In the free molecule regime ($l/a \gg 1$), the velocity distribution of the incoming gas molecules may be taken to be uninfluenced by the small particle and given by the Maxwell or Chapman–Enskog distributions (Waldmann and Schmitt, 1966; Whitmore, 1981). Under this assumption, the thermophoretic mobility was found to be

$$A = \frac{3\eta}{4(1+\pi\beta_t/8)\rho_f T_0} \tag{2}$$

where η is the fluid viscosity, ρ_f is the fluid density, and T_0 is the bulk gas absolute temperature at the particle center in the absence of the particle (or the mean gas temperature in the vicinity of the particle). The theory adopts the usual assumption that a fraction β_t of the gas molecules colliding with the particle is reflected diffusely (thermally) with a Maxwellian distribution and the remaining fraction $(1-\beta_t)$ is reflected specularly. The value of the coefficient of diffuse reflection (β_t) is usually about 0.9 (Friedlander, 1977). Note that $\rho_f T_0$ is constant for an ideal gas at constant pressure and the thermophoretic mobility for the "small particle" regime is independent of particle size.

In the "large particle" regime ($l/a \ll 1$), the fluid flow may be described by a continuum model and the thermophoretic force arises from an induced thermal slip along the particle surface due to the existence of a tangential temperature gradient at the particle–fluid interface. On the basis of the assumptions of small thermal Peclet number and small Reynolds number as well as the effects of temperature jump, thermal slip, and frictional slip at the particle surface, Brock (1962) obtained the thermophoretic mobility of an aerosol sphere as

$$A = \left[\frac{2C_s(k+k_1C_t l/a)}{(1+2C_m l/a)(2k+k_1+2kC_t l/a)}\right]\frac{\eta}{\rho_f T_0} \tag{3}$$

In Eq. 3, k and k_1 are the thermal conductivities of the gas and of the particle, respectively; C_s, C_t, and C_m are dimensionless coefficients accounting for the thermal slip, temperature jump, and frictional slip phenomena, respectively, at the particle surface and must be determined experimentally for each gas–solid system. A set of reasonable kinetic-theory values for perfect energy and momentum accommodations appear to be $C_s = 1.17$, $C_t = 2.18$, and $C_m = 1.14$ (Talbot et al., 1980). It has been shown that Eqs. 1 and 3 with no particle rotation holds even if ∇T_∞ varies appreciably over length scales comparable to the particle radius, with ∇T_∞ evaluated at the position of the particle center (Keh and Chen, 1995).

Recently, the thermophoretic force on single aerosol spheres was measured over a wide range of Knudsen numbers and particle thermal conductivities (Li and Davis, 1995). It was found that the data in the transition regime [$l/a = O(1)$] overlap Loyalka's (1992) solution of the linearized Boltzmann equation for hard-sphere molecules, and the data in the slip regime agree with Brock's results of Eq. 3.

In practical applications of thermophoresis, aerosol particles usually are not isolated and will move in the presence of neighboring particles and/or boundaries. Through the use of a boundary collocation technique, the quasi-steady thermophoretic motion of an aerosol sphere in the direction perpendicular to a plane wall was semianalytically examined (Chen and Keh, 1995). Numerical results of correction to Eq. 3 for the particle were presented for various cases. Later, analytical solutions for the thermophoretic mobility of a sphere near a plane wall in asymptotic forms were obtained by using a method of reflections (Chen, 2000). On the other hand, the quasi-steady thermophoresis of an aerosol sphere in a spherical cavity has been investigated (Keh and Chang, 1998; Lu and Lee, 2001). An analytical expression for the wall-corrected velocity of the particle located at the center of the cavity was derived in a closed form.

The purpose of this article is to obtain exact numerical solutions and approximate analytical solutions for the thermophoretic motions of a spherical particle parallel to a single plane wall and to two plane walls at an arbitrary position between them. The plane walls may be either insulated or prescribed with the linear far-field temperature distribution. The effects of fluid inertia as well as thermal convection are neglected. For the case of a particle with a relatively low thermal conductivity undergoing thermophoresis near insulated plane walls or of a particle with a relatively high conductivity undergoing thermophoresis near plane walls prescribed with the far-field temperature distribution, the heat conduction around the particle will generate larger temperature gradients on the particle surface relative to those in an infinite medium. These gradients enhance the thermophoretic velocity, although their action will be retarded by the viscous interaction of the migrating particle with the walls. Both effects of this thermal enhancement and the hydrodynamic retardation increase as the ratios of the radius of the particle to its distances from the walls increase. Determining which effect is overriding at small particle-wall gap widths is a main target of this study.

Analysis

We consider the steady thermophoresis of a rigid spherical particle of radius a in a gaseous medium parallel to two infinite plane walls whose distances from the center of the particle are b and c, as shown in Figure 1. Here (x,y,z), (ρ,ϕ,z), and (r,θ,ϕ) denote the rectangular, circular cylindrical, and spherical coordinate systems, respectively, and the origin of coordinates is chosen at the particle center. A linear temperature field $T_\infty(\boldsymbol{x})$ with a uniform thermal gradient $-E_\infty \boldsymbol{e}_x$ (=

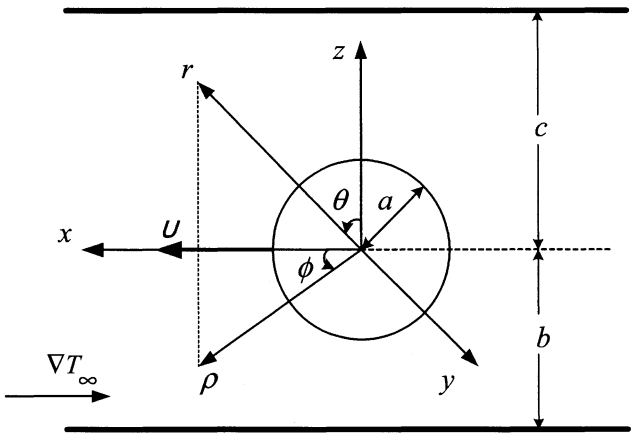

Figure 1. Geometrical sketch for the thermophoresis of a spherical particle parallel to two plane walls at an arbitrary position between them.

∇T_∞, where E_∞ is taken to be positive) is imposed in the surrounding fluid far away from the particle, where $\boldsymbol{x}$ is the position vector and $\boldsymbol{e}_x$ together with $\boldsymbol{e}_y$ and $\boldsymbol{e}_z$ are the unit vectors in rectangular coordinates. It is assumed that the Knudsen number l/a is small, so that the fluid flow is in the continuum regime and the Knudsen layer at the particle surface is thin in comparison with the radius of the particle and the spacing between the particle and each wall. The objective is to determine the correction to Eq. 3 for the particle mobility due to the presence of the plane walls.

Before determining the thermophoretic velocity of the particle, the velocity field in the fluid phase needs to be found. Because the boundary condition of the velocity field is coupled with the temperature gradient at the particle surface, it is necessary to determine the temperature distribution first.

Temperature distribution

The thermal Peclet number of the steady system is assumed to be small. Hence, the equation of energy governing the temperature distribution $T(\boldsymbol{x})$ for the fluid phase of constant thermal conductivity k is the Laplace equation

$$\nabla^2 T = 0 \quad (r \geq a) \tag{4a}$$

For the temperature field $T_1(\boldsymbol{x})$ inside the particle, one has

$$\nabla^2 T_1 = 0 \quad (r \leq a) \tag{4b}$$

The boundary conditions at the particle surface require that the normal component of heat flux be continuous and a temperature jump that is proportional to the normal temperature gradient (Kennard, 1938) occur. Thus

$$r = a: \qquad k\frac{\partial T}{\partial r} = k_1\frac{\partial T_1}{\partial r} \tag{5a}$$

$$T - T_1 = C_t l\frac{\partial T}{\partial r} \tag{5b}$$

where k_1 is the thermal conductivity of the particle, and C_t is the temperature jump coefficient about the surface of the particle; both are assumed to be constant.

The temperature far away from the particle approaches the undisturbed values. We can write

$$z = c, -b: \qquad \frac{\partial T}{\partial z} = 0 \tag{6}$$

$$\rho \to \infty: \qquad T \to T_\infty = T_0 - E_\infty x \tag{7}$$

Note that the boundary conditions given by Eq. 6 apply for the case of two insulated plane walls. For the case of thermophoretic motion of a particle parallel to two plane walls prescribed with a linear temperature profile consistent with the far-field distribution, Eq. 6 should be replaced by

$$z = c, -b: \quad T = T_0 - E_\infty x \tag{8}$$

Since the governing equation and boundary conditions are linear, one can express the external temperature distribution, T, which is symmetric with respect to y and antisymmetric with respect to x, as the superposition

$$T = T_w + T_p \tag{9}$$

Here, T_w is a double Fourier integral solution of Eq. 4a in rectangular coordinates that represents the disturbance produced by the plane walls plus the undisturbed temperature field, and is given by

$$T_w = T_0 - E_\infty x - E_\infty \int_0^\infty \int_0^\infty (Xe^{\kappa z} + Ye^{-\kappa z})\sin(\alpha x) \times \cos(\beta y)\, d\alpha\, d\beta \tag{10}$$

where X and Y are unknown functions of separation variables α and β, and $\kappa = (\alpha^2 + \beta^2)^{1/2}$. The second term on the righthand side of Eq. 9, T_p, is a solution of Eq. 4a in spherical coordinates representing the disturbance generated by the particle, and is given by an infinite series in harmonics,

$$T_p = -E_\infty \sum_{n=1}^{\infty} R_n r^{-n-1} P_n^1(\mu)\cos\phi \tag{11}$$

where P_n^1 is the associated Legendre function of the order n and degree one, μ is used to denote $\cos\theta$ for brevity, and R_n are unknown constants. Note that a solution for T of the form given by Eqs. 9–11 immediately satisfies the boundary condition at infinity in Eq. 7. Since the temperature is finite for any position in the interior of the particle, the solution to Eq. 4b can be written as

$$T_1 = T_0 - E_\infty \sum_{n=1}^{\infty} \bar{R}_n r^n P_n^1(\mu)\cos\phi \tag{12}$$

where $\bar{R}_n$ are unknown constants.

Substituting the temperature distribution T given by Eqs. 9–11 into the boundary conditions in Eq. 6 or 8, and applying the Fourier sine and cosine transforms on the variables x and y, respectively, lead to a solution for the functions X and Y in terms of the coefficients R_n. After the substitution of this solution into Eq. 10 and utilization of the integral representations of the modified Bessel functions of the second kind, the temperature distribution, T, can be expressed as

$$T = T_0 - E_\infty x - E_\infty \sum_{n=1}^{\infty} R_n \delta_n^{(1)}(r,\mu)\cos\phi \tag{13}$$

where the function $\delta_n^{(1)}(r,\mu)$ is defined by Eq. B1 in Appendix B.

Applying the boundary conditions given by Eq. 5 to Eqs. 12 and 13 yields

$$\sum_{n=1}^{\infty} \left[R_n \delta_n^{(2)}(a,\mu) - \overline{R}_n k^* n a^{n-1} P_n^1(\mu) \right] = -\left(1-\mu^2\right)^{1/2} \tag{14a}$$

$$\sum_{n=1}^{\infty} \left\{ R_n \left[\delta_n^{(1)}(a,\mu) - aC_t^* \delta_n^{(2)}(a,\mu) \right] - \overline{R}_n a^n P_n^1(\mu) \right\} = -a(1-C_t^*)\left(1-\mu^2\right)^{1/2} \tag{14b}$$

where $k^* = k_1/k$, $C_t^* = C_t l/a$, and the definition of the function $\delta_n^{(2)}(r,\mu)$ is given by Eq. B2. Note that the dependence on ϕ factors out in Eq. 14 and the definite integrals in $\delta_n^{(1)}$ and $\delta_n^{(2)}$ must be performed numerically.

To satisfy the condition in Eq. 14 exactly along the entire surface of the particle would require the solution of the entire infinite array of unknown constants, R_n and $\overline{R}_n$. However, the collocation method (O'Brien, 1968; Ganatos et al., 1980; Chen and Keh, 1995) enforces the boundary conditions at a finite number of discrete points on the half-circular generating arc of the sphere (from $\theta = 0$ to $\theta = \pi$) and truncates the infinite series in Eqs. 12 and 13 into finite ones. If the spherical boundary is approximated by satisfying the conditions of Eq. 5 at M discrete points on its generating arc, the infinite series in Eqs. 12 and 13 are truncated after M terms, resulting in a system of $2M$ simultaneous linear algebraic equations in the truncated form of Eq. 14. This matrix equation can be numerically solved to yield the $2M$ unknown constants R_n and $\overline{R}_n$ required in the truncated form of Eqs. 12 and 13 for the temperature distribution. The accuracy of the boundary–collocation/truncation technique can be improved to any degree by taking a sufficiently large value of M. Naturally, as $M \to \infty$, the truncation error vanishes and the overall accuracy of the solution depends only on the numerical integration required in evaluating the matrix elements.

Fluid velocity distribution

With knowledge of the solution for the temperature distribution on the particle surface, which drives the thermophoretic migration, we can now proceed to find the flow field. The fluid is assumed to be incompressible and Newtonian. Owing to the low Reynolds number, the fluid motion caused by the thermophoresis of the particle is governed by the Stokes equations

$$\eta \nabla^2 \boldsymbol{v} - \nabla p = \boldsymbol{0} \tag{15a}$$

$$\nabla \cdot \boldsymbol{v} = 0 \tag{15b}$$

where $\boldsymbol{v}(\boldsymbol{x})$ is the velocity field for the fluid flow and $p(\boldsymbol{x})$ is the dynamic pressure distribution.

The boundary conditions for the fluid velocity at the particle surface (Brock, 1962), on the plane walls, and far removed from the particle are

$$r = a: \qquad \boldsymbol{v} = \boldsymbol{U} + a\boldsymbol{\Omega} \times \boldsymbol{e}_r + \frac{C_m l}{\eta}(\boldsymbol{I} - \boldsymbol{e}_r\boldsymbol{e}_r)\boldsymbol{e}_r : \boldsymbol{\tau} + C_s \frac{\eta}{\rho_f T_0}(\boldsymbol{I} - \boldsymbol{e}_r\boldsymbol{e}_r)\cdot\nabla T \tag{16}$$

$$z = c, -b: \qquad \boldsymbol{v} = \boldsymbol{0} \tag{17}$$

$$\rho \to \infty: \qquad \boldsymbol{v} = \boldsymbol{0} \tag{18}$$

Here, $\boldsymbol{\tau} = \eta[\nabla \boldsymbol{v} + (\nabla \boldsymbol{v})^T]$ is the viscous stress tensor for the fluid; $\boldsymbol{e}_r$, together with $\boldsymbol{e}_\theta$ and $\boldsymbol{e}_\phi$, are the unit vectors in spherical coordinates; $\boldsymbol{I}$ is the unit dyadic; C_m and C_s are the frictional and thermal slip coefficients, respectively, about the surface of the particle; and $\boldsymbol{U} = U\boldsymbol{e}_x$ and $\boldsymbol{\Omega} = \Omega \boldsymbol{e}_y$ are the translational and angular velocities of the particle undergoing thermophoresis to be determined. For the asymmetric problem as $b \neq c$, the assumption that the sphere would migrate in a direction parallel to the temperature gradient is justified in the absence of inertia. Note that the possible thermoosmotic flow caused by the plane walls is ignored.

A fundamental solution to Eq. 15, which satisfies Eqs. 17 and 18, can be constructed by the procedure used in the previous subsection for the solution of the temperature field and expressed as

$$\boldsymbol{v} = v_x \boldsymbol{e}_x + v_y \boldsymbol{e}_y + v_z \boldsymbol{e}_z \tag{19}$$

where

$$v_x = \sum_{n=1}^{\infty} \left[A_n(A_n' + \alpha_n') + B_n(B_n' + \beta_n') + C_n(C_n' + \gamma_n') \right] \tag{20a}$$

$$v_y = \sum_{n=1}^{\infty} \left[A_n(A_n'' + \alpha_n'') + B_n(B_n'' + \beta_n'') + C_n(C_n'' + \gamma_n'') \right] \tag{20b}$$

$$v_z = \sum_{n=1}^{\infty} \left[A_n(A_n''' + \alpha_n''') + B_n(B_n''' + \beta_n''') + C_n(C_n''' + \gamma_n''') \right] \tag{20c}$$

Here, the primed A_n, B_n, C_n, α_n, β_n, and γ_n are functions of the position involving associated Legendre functions of μ or $\cos\theta$ defined by Eq. 2.6 and in the form of integration (which must be performed numerically) defined by Eq. C1 of Ganatos et al. (1980), and A_n, B_n, and C_n are unknown constants.

The boundary condition that remains to be satisfied is that on the particle surface. Substituting Eqs. 13 and 19 into Eq. 16, one obtains

$$\sum_{n=1}^{\infty}\left[A_nA_n^*(a,\mu,\phi)+B_nB_n^*(a,\mu,\phi)+C_nC_n^*(a,\mu,\phi)\right]=U(1-\mu^2)^{1/2}\cos\phi \quad (21a)$$

$$\sum_{n=1}^{\infty}\left[A_nA_n^{**}(a,\mu,\phi)+B_nB_n^{**}(a,\mu,\phi)+C_nC_n^{**}(a,\mu,\phi)\right]-C_m^*\sum_{n=1}^{\infty}\left\{\left(r\frac{\partial}{\partial r}-1\right)\left[A_nA_n^{**}(r,\mu,\phi)+B_nB_n^{**}(r,\mu,\phi)+C_nC_n^{**}(r,\mu,\phi)\right]-(1-\mu^2)^{1/2}\frac{\partial}{\partial\mu}\left[A_nA_n^*(r,\mu,\phi)+B_nB_n^*(r,\mu,\phi)+C_nC_n^*(r,\mu,\phi)\right]\right\}_{r=a}=U\mu\cos\phi+a\Omega\cos\phi-C_s\frac{\eta E_\infty}{\rho_fT_0}\left[\mu+\frac{1}{a}\sum_{n=1}^{\infty}R_n\delta_n^{(3)}(a,\mu)\right]\cos\phi \quad (21b)$$

$$\sum_{n=1}^{\infty}\left[A_nA_n^{***}(a,\mu,\phi)+B_nB_n^{***}(a,\mu,\phi)+C_nC_n^{***}(a,\mu,\phi)\right]-C_m^*\left[\sum_{n=1}^{\infty}\left\{\left(r\frac{\partial}{\partial r}-1\right)\left[A_nA_n^{***}(r,\mu,\phi)+B_nB_n^{***}(r,\mu,\phi)+C_nC_n^{***}(r,\mu,\phi)\right]+(1-\mu^2)^{-1/2}\frac{\partial}{\partial\phi}\left[A_nA_n^*(r,\mu,\phi)+B_nB_n^*(r,\mu,\phi)+C_nC_n^*(r,\mu,\phi)\right]\right\}_{r=a}=-U\sin\phi-a\Omega\mu\sin\phi+C_s\frac{\eta E_\infty}{\rho_fT_0}\left[(1-\mu^2)^{1/2}+\frac{1}{a}\sum_{n=1}^{\infty}R_n\delta_n^{(1)}(a,\mu)\right]\sin\phi \quad (21c)$$

where $C_m^*=C_ml/a$; the function $\delta_n^{(3)}(r,\mu)$ is defined by Eq. B3; and the definitions of the starred A_n, B_n, and C_n functions are given by Eq. B6. The first $2M$ coefficients R_n and $\overline{R}_n$ have been determined through the procedure given in the previous subsection.

Careful examination of Eq. 21 shows that the solution of the coefficient matrix generated is independent of the ϕ coordinate of the boundary points on the surface of the sphere $r=a$. Thus, these relations can be satisfied by utilizing the collocation technique presented for the solution of the temperature field. At the particle surface, Eq. 21 is applied at N discrete points (values of θ between 0 and π) and the infinite series in Eq. 20 are truncated after N terms. This generates a set of $3N$ linear algebraic equations for the $3N$ unknown coefficients A_n, B_n, and C_n. The fluid velocity field is completely obtained once these coefficients are solved for a sufficiently large value of N.

Derivation of the particle velocities

The drag force and torque exerted by the fluid on the spherical particle can be determined from (Ganatos et al., 1980)

$$\boldsymbol{F}=-8\pi\eta A_1\boldsymbol{e}_x \quad (22a)$$

$$\boldsymbol{T}=-8\pi\eta C_1\boldsymbol{e}_y \quad (22b)$$

These expressions show that only the lowest-order coefficients A_1 and C_1 contribute to the hydrodynamic force and couple acting on the particle.

Because the particle is freely suspended in the surrounding fluid, the net force and torque exerted on the particle must vanish. Applying this constraint to Eq. 22, one has

$$A_1=C_1=0 \quad (23)$$

To determine the translational and angular velocities U and Ω of the particle, Eq. 23 and the $3N$ algebraic equations resulting from Eq. 21 are to be solved simultaneously. Note that, similar to the thermophoretic velocity of an isolated sphere given by Eqs. 1 and 3, both values of U and Ω are proportional to the quantity $C_s\eta E_\infty/\rho_fT_0$ and dependent on the dimensionless parameters k^*, C_t^*, and C_m^* (in addition to the length ratios among a, b, and c).

Results and Discussion

The solution for the thermophoretic motion of a spherical particle parallel to two plane walls at an arbitrary position between them, obtained by using the boundary collocation method described in the previous section, is presented in this section. The system of linear algebraic equations to be solved for the coefficients R_n and $\overline{R}_n$ is constructed from Eq. 14, while that for A_n, B_n, and C_n is composed of Eq. 21. All the numerical integrations to evaluate the primed α_n, β_n, and γ_n as well as $\delta_n^{(i)}$ functions were done by the 80-point Gauss–Laguerre quadrature.

When specifying the points along the semicircular generating arc of the sphere (with a constant value of ϕ), where the boundary conditions are to be exactly satisfied, the first points that should be chosen are $\theta=0$ and π, since these points define the projected area of the particle normal to the direction of motion and control the gaps between the particle and the neighboring plates. In addition, the point $\theta=\pi/2$ is also important. However, an examination of the systems of linear algebraic equations in Eqs. 14 and 21 shows that the matrix equations become singular if these points are used. To overcome this difficulty, these points are replaced by closely adjacent points, that is, $\theta=\delta$, $\pi/2-\delta$, $\pi/2+\delta$, and $\pi-\delta$ (Ganatos et al., 1980). Additional points along the boundary are selected as mirror-image pairs about the plane $\theta=\pi/2$ to divide the two quarter-circular arcs of the particle into equal segments. The optimum value of δ in this work is found to be 0.1°, with which the numerical results of the particle velocities converge satisfactorily. In selecting the boundary points, any value of ϕ can be used, except for $\phi=0$, $\pi/2$, and π, since the coefficient matrix in Eq. 21 is singular for these values.

For the continuum-with-slippage approach employed in this work, the Knudsen number (l/a) of the system should be smaller than about 0.1. As mentioned in the first section, a set of well-adapted values for the temperature jump and frictional slip coefficients under the condition of complete ther-

mal and momentum accommodations are 2.18 and 1.14, respectively. Consequently, the normalized coefficients C_t^* and C_m^* must be restricted to be less than unity. For convenience we will use the ratio $C_t^*/C_m^* = 2$ (a rounded value to $2.18/1.14 = 1.91$) throughout this section, without the loss of reality or generality. On the other hand, the thermal conductivity of an aerosol particle is usually greater than that of the surrounding gas. Thus, the value of the relative conductivity, k^*, will exceed unity under most practical circumstances.

Motion parallel to a single plane wall

The collocation solutions for the translational and rotational velocities of a spherical particle with $C_t^* = C_m^* = 0$ undergoing thermophoresis parallel to a plane wall (that is, with $c \to \infty$) for different values of the parameters k^* and a/b are presented in Tables 1 and 2 for the cases of an insulated wall and a wall with the imposed far-field temperature gradient, respectively. The velocity for the thermophoretic motion of an identical particle in an infinite fluid, $U_0 = AE_\infty$, given by Eqs. 1 and 3, is used to normalize the boundary-corrected values. Thus, the normalized particle velocities are independent of the values of C_s, E_∞, η, and $\rho_f T_0$. The limiting case of $k^* = 0$, which is not likely to exist in practice, is considered here for the sake of numerical comparison. All of the results obtained under the collocation scheme converge satisfactorily to at least the significant figures shown in the tables. The accuracy and convergence behavior of the truncation technique is principally a function of the ratio a/b. For the most difficult case with $a/b = 0.999$, the numbers of collocation points $M = 36$ and $N = 36$ are sufficiently large to achieve this convergence.

In Appendix A, an approximate analytical solution for the same thermophoretic motion as that considered here is also obtained by using a method of reflections. The translational and angular velocities of a spherical particle near a lateral plate is given by Eqs. A11a and A11b, which are power-series expansions in λ ($= a/b$). The values of the wall-corrected normalized particle velocities calculated from this asymptotic solution, with the $O(\lambda^8)$ term neglected, are also listed in Tables 1 and 2 for comparison. It can be seen that the asymptotic formula of Eq. A11a from the method of reflections for U/U_0 agrees very well with the exact results as long as $\lambda \le 0.8$; the errors in all cases are less than 1.3%. However, the accuracy of Eqs. A11a and A11b [especially of Eq. A11b for $a\Omega/U_0$, in which the leading term is $O(\lambda^4)$], deteriorates rapidly, as expected, when the relative spacing between the particle and the plane wall becomes small.

The exact numerical solutions for the normalized velocities U/U_0 and $a\Omega/U_0$ of a spherical particle with $C_t^* = 2C_m^* = 0.02$ undergoing thermophoresis parallel to a plane wall as functions of a/b are depicted in Figure 2 for various values of k^*. It is evident that the wall-corrected normalized thermophoretic mobility U/U_0 of the particle decreases with an increase in k^* for the case of an insulated wall (the boundary condition Eq. 6 is used), but increases with an increase in k^* for the case of a plane wall prescribed with the far-field temperature distribution (the boundary condition Eq. 8 is used), keeping the other factors (C_t^*, C_m^*, and a/b) unchanged. This decrease and increase in the particle mobility becomes more pronounced as a/b increases. This behavior is expected, knowing that the temperature gradients on the particle surface near an insulated wall decrease as the relative conductivity k^* increases and these gradients near a wall with the imposed far-field temperature gradient increase as k^* increases (see the analysis in Appendix A). When $k^* = (1-$

Table 1. Normalized Translational and Rotational Velocities of a Spherical Particle Undergoing Thermophoresis Parallel to a Single Insulated Plane Wall with $C_t^* = C_m^* = 0$*

	U/U_0		$-a\Omega/U_0$	
a/b	Exact Solution	Asymptotic Solution	Exact Solution	Asymptotic Solution
		$k^* = 0$		
0.2	0.99953	0.99953	0.00030	0.00030
0.4	0.99684	0.99678	0.00492	0.00493
0.6	0.99172	0.99057	0.02669	0.02660
0.8	0.98853	0.97722	0.10164	0.09400
0.9	0.99789	0.96390	0.20389	0.16225
0.95	1.0223	0.95412	0.3189	0.21001
0.99	1.1450	0.94422	0.6162	0.25657
0.995	1.231		0.759	
0.999	1.440		1.063	
		$k^* = 10$		
0.2	0.99828	0.99828	0.00030	0.00030
0.4	0.98640	0.98636	0.00498	0.00500
0.6	0.95251	0.95202	0.02759	0.02776
0.8	0.86845	0.87022	0.10766	0.10275
0.9	0.77441	0.79527	0.21183	0.18221
0.95	0.6864	0.74447	0.3119	0.23914
0.99	0.5324	0.69568	0.4778	0.29545
0.995	0.492		0.520	
0.999	0.449		0.559	

*Computed from the Exact Boundary–Collocation Solution and the Asymptotic Method-of-Reflection Solution

Table 2. Normalized Translational and Rotational Velocities of a Spherical Particle Undergoing Thermophoresis Parallel to a Single Plane Wall Prescribed with the Far-Field Temperature Profile with $C_t^* = C_m^* = 0$*

	U/U_0		$-a\Omega/U_0$	
a/b	Exact Solution	Asymptotic Solution	Exact Solution	Asymptotic Solution
		$k^* = 0$		
0.2	0.99853	0.99853	0.00030	0.00030
0.4	0.98840	0.98837	0.00498	0.00500
0.6	0.95922	0.95883	0.02767	0.02774
0.8	0.88358	0.88659	0.10880	0.10261
0.9	0.79405	0.81880	0.21593	0.18187
0.95	0.7070	0.77229	0.3200	0.23865
0.99	0.5509	0.72732	0.4940	0.29480
0.995	0.510		0.538	
0.999	0.465		0.580	
		$k^* = 10$		
0.2	0.99978	0.99978	0.00030	0.00030
0.4	0.99888	0.99883	0.00492	0.00493
0.6	0.99907	0.99784	0.02676	0.02658
0.8	1.00890	0.99614	0.10276	0.09386
0.9	1.03209	0.99261	0.20872	0.16192
0.95	1.0678	0.98912	0.3312	0.20952
0.99	1.1836	0.98506	0.6613	0.25592
0.995	1.247		0.817	
0.999	1.391		1.105	

*Computed from the Exact Boundary–Collocation Solution and the Asymptotic Method-of-Reflection Solution

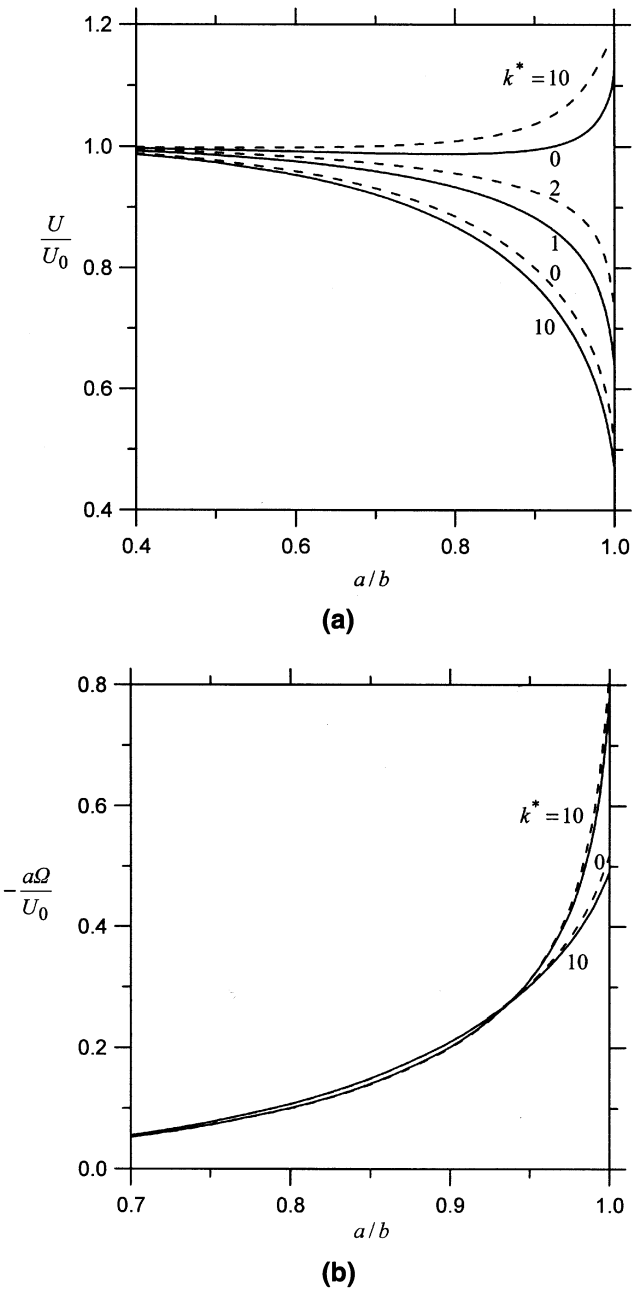

Figure 2. Normalized velocities of a spherical particle with $C_t^* = 2C_m^* = 0.02$ undergoing thermophoresis parallel to a plane wall vs. separation parameter a/b for values of k^*.

(a) Translational velocity U/U_0; (b) rotational velocity $a\Omega/U_0$. The solid curves represent the case of an insulated wall, and the dashed curves denote the case of a wall on which the far-field temperature gradient is imposed.

$C_t^*)^{-1}$, the two types of plane wall will result in the same effects on the thermophoretic motion of the particle. In this particular case, the effect of thermal interaction between the particle and the wall disappears, and the relative thermophoretic mobility of the particle decreases monotonically with a/b solely owing to the hydrodynamic resistance exerted by the presence of the wall.

Examination of the results shown in Tables 1 and 2 and Figure 2a reveals an interesting feature when the particle has small values of C_t^* and C_m^*. For the case that the wall is an insulated plane under the situation of small k^* (such as with $k^* = 0$), the thermophoretic mobility of the particle decreases with an increase in a/b, as a/b is small, but increases from a minimum with increasing a/b, as a/b is sufficiently large. When the gap between the particle and the wall turns thin, the particle can even move faster than it would at $a/b = 0$. For example, as $C_t^* = C_m^* = 0$, $k^* = 0$, and $a/b = 0.999$, the thermophoretic velocity can be as much as 45% higher than the value with the wall that is far away from the particle. Under the situations of relatively large k^*, the thermophoretic mobility of the particle near the insulated wall is a monotonically decreasing function of a/b. For the case that a linear temperature profile is prescribed on the plane wall, which is consistent with the far-field distribution under the situation of large k^* (such as with $k^* = 10$), the thermophoretic mobility of the particle first goes through a minimum with the increase of a/b from $a/b = 0$ and then increases monotonically. Again, the value of U/U_0 can be greater than unity when $a/b \to 1$. Under the situation of relatively small k^*, the thermophoretic mobility of the particle near the wall prescribed with the far-field temperature distribution becomes a monotonically decreasing function of a/b. This interesting feature that U/U_0 may not be a monotonic function of a/b and can even be greater than unity is understandable, because the wall effect of hydrodynamic resistance on the particle is in competition with the wall effect of thermal enhancement when a particle with small k^* is undergoing thermophoretic motion parallel to an insulated plate or when a particle with large k^* is moving near a lateral plate with the imposed far-field temperature gradient. A careful examination of the asymptotic formula for U/U_0 given by Eq. A11a shows the good agreement of the numerical outcome in Figure 2a with the analytical solution.

The results in Tables 1 and 2 and Figure 2b indicate that the spherical particle undergoing thermophoresis parallel to a plane wall rotates in the direction opposite to that for a sphere migrating in the same direction but under a body–force field (such as a gravitational field (O'Neill, 1964)). The explanation for this behavior is analogous to the case of electrophoresis of a charged sphere with a thin electric double layer parallel to a nonconducting plate (Keh and Chen, 1988). For any specified values of C_t^*, C_m^*, and k^*, the magnitude of the normalized rotational velocity of the thermophoretic sphere near a given plane wall is a monotonically increasing function of a/b. For a fixed value of a/b not close to unity, the magnitude of $a\Omega/U_0$ is not a sensitive function of k^*. On the other hand, for a given value of a/b close to unity, the magnitude of $a\Omega/U_0$ decreases with an increase in k^* for the thermophoresis of a particle with constant values of C_t^* and C_m^* parallel to an insulated plate, but increases with an increase in k^* for the migration parallel to a wall prescribed with the far-field temperature profile.

Figures 3a and 3b show the effect of a variation in C_t^* ($= 2C_m^*$, proportional to the Knudsen number, l/a) on the wall-corrected normalized particle velocities, U/U_0 and $a\Omega/U_0$, respectively, for the case of $k^* = 100$. It can be seen that there exist extreme points along the curves for both velocities. For the case of an insulated plane wall, U/U_0 in-

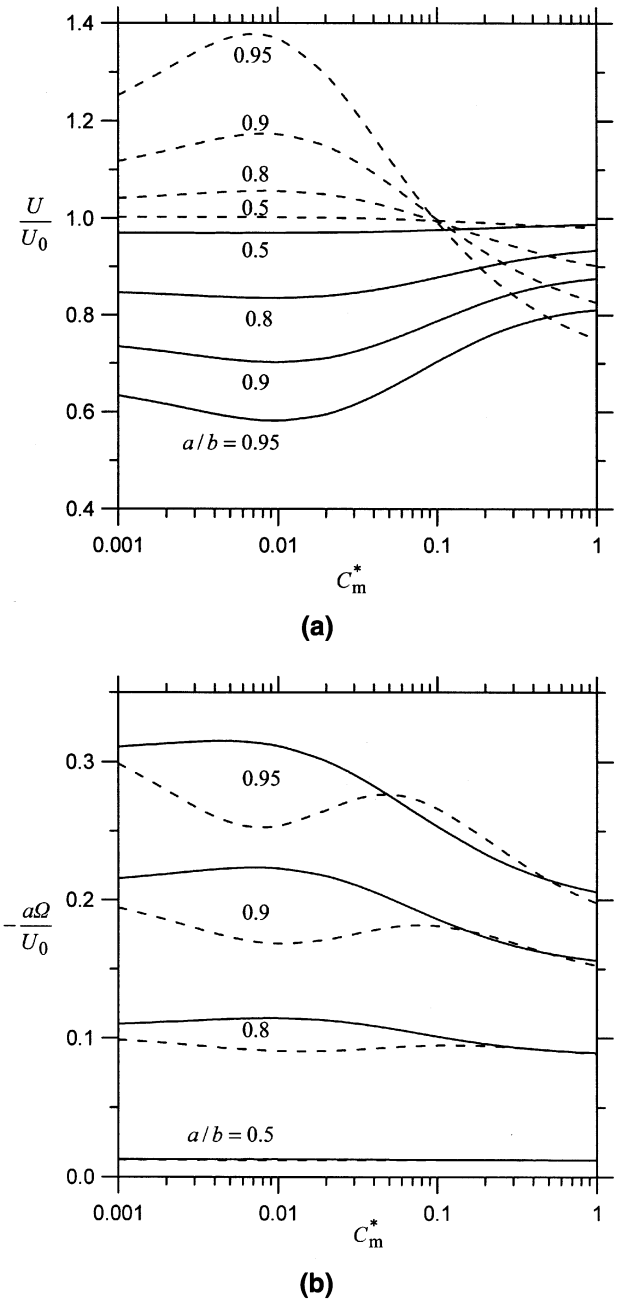

Figure 3. Normalized velocities of a spherical particle with $C_t^* = 2C_m^*$ and $k^* = 100$ undergoing thermophoresis parallel to a plane wall vs. normalized frictional slip coefficient for values of the separation parameter a/b.

(a) Translational velocity U/U_0; (b) rotational velocity $a\Omega/U_0$. The solid curves represent the case of an insulated wall, and the dashed curves denote the case of a wall on which the far-field temperature gradient is imposed.

creases with an increase in C_t^*, but decreases with the accompanying increase in C_m^*, and the competition between these two opposite effects results in a minimum of U/U_0. On the other hand, for the case of a plane wall prescribed with a linear temperature profile consistent with the far-field distribution, U/U_0 drops with an increase in C_t^*, but grows with the simultaneous increase in C_m^*, and the net effect leads to a maximum (whose value can be much greater than unity, since k^* is large in the present case). In general, these extreme points occur in the vicinity of $C_m^* = 0.01$.

The effect of varying the relative thermal conductivity k^* on the wall-corrected normalized particle velocities U/U_0 and $a\Omega/U_0$ is illustrated in Figures 4a and 4b, respectively, for the case of $C_t^* = 2C_m^* = 0.2$. As expected, the curves for U/U_0 vs. k^* show a monotonically decreasing tendency for the case of an insulated plane wall and a monotonically increasing trend for the case of a plane wall imposed with the far-field temperature profile. However, the value of U/U_0 may no longer be greater than unity in this case (with relatively large values of C_t^* and C_m^*). Again, the value of $a\Omega/U_0$ is not a sensitive function of k^* for most values of a/b.

For the creeping motion of a free-rotating spherical aerosol particle with a frictional (but isothermal) slip surface on which a constant body force $\boldsymbol{Fe}_x$ (such as a gravitational field) is exerted parallel to an infinite plane wall, the exact result of the particle velocity has recently been developed by using the boundary-collocation technique (Chen and Keh, 2003). A comparison of the boundary effects on the motion of the aerosol sphere under gravity (in which $U_0 = (F/6\pi\eta a)(1 + 3C_m^*)/(1 + 2C_m^*)$) and on the thermophoresis is given in Figure 5. Obviously, the wall effect on thermophoretic motion is much weaker than that on a sedimenting particle. Note that the wall effect on the particle motion in a gravitational field is stronger when the value of C_m^* becomes smaller, which is opposite to that which would occur if a particle with a relatively large value of C_m^* migrates near a plane wall due to a thermophoretic driving force.

Motion parallel to two plane walls

The converged collocation solutions for the normalized velocity U/U_0 of a spherical particle with $C_t^* = C_m^* = 0$ undergoing thermophoresis on the median plane between two parallel plane walls (with $c = b$ and $\Omega = 0$) for various values of the parameters k^* and a/b are presented in Table 3 for both cases of insulated walls and walls prescribed with the far-field temperature distribution. The corresponding method-of-reflection soultions, given by Eq. A20 in Appendix A as a power series expansion in $\lambda (= a/b)$ correct to $O(\lambda^7)$, are also listed in this table for comparison. Similar to the case of the migration of a spherical particle parallel to a single plane wall considered in the previous subsection, the approximate analytical formula of Eq. A20 agrees very well with the exact results as long as $\lambda \le 0.6$, but can have significant errors when $\lambda \ge 0.8$. In general, Eq. A20 overestimates the thermophoretic velocity of the particle. A comparison between Table 3 for the case of a slit and Tables 1 and 2 for the case of a single parallel plane indicates that the assumption that the boundary effect for two walls can be obtained by simple addition of single-wall effects leads to a smaller correction to thermophoretic motion as a/b is small, but can give a greater correction as a/b becomes large.

In Figure 6, the collocation results for the normalized thermophoretic mobility U/U_0 of a sphere migrating on the median plane between two parallel plane walls are plotted as functions of a/b for two related sets of C_t^* and C_m^* and several values of k^*. Analogous to the corresponding motion of

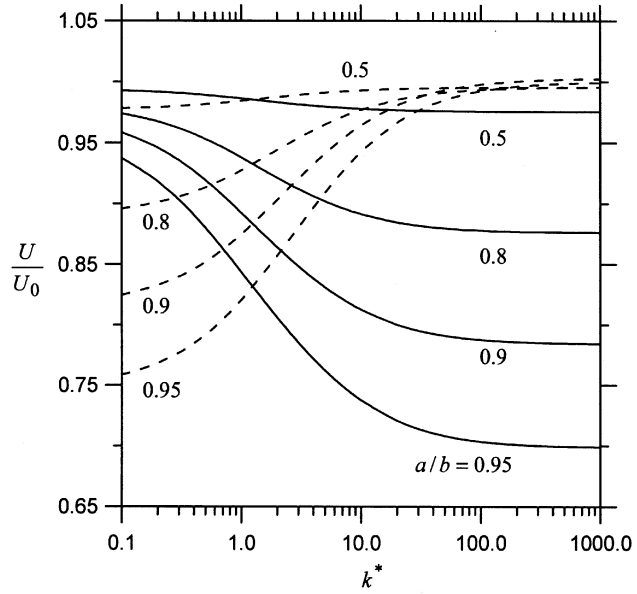

(a)

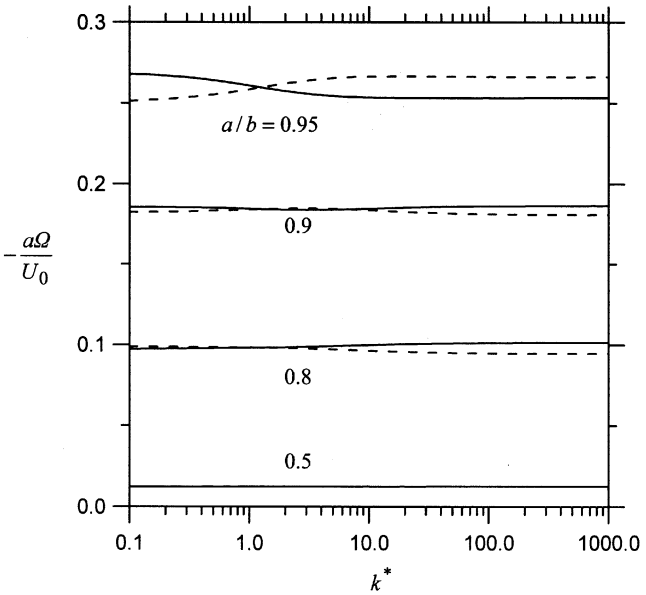

(b)

Figure 4. Normalized velocities of a spherical particle with $C_t^* = 2C_m^* = 0.2$ undergoing thermophoresis parallel to a plane wall vs. relative thermal conductivity of the particle for values of the separation parameter *a/b*.

(a) Translational velocity U/U_0; (b) rotational velocity $a\Omega/U_0$. The solid curves represent the case of an insulated wall, and the dashed curves denote the case of a wall on which the far-field temperature gradient is imposed.

a particle parallel to a single plane wall, for specified values of C_t^*, C_m^*, and a/b, U/U_0 increases with an increase in k^* for the case of walls with the imposed far-field temperature gradient and decreases with an increase in k^* for the case of insulated walls. Again, as shown in Figure 6a with small values of C_t^* and C_m^*, for the case of insulated walls under the situation of small k^*, or for the case of walls prescribed with the far-field temperature distribution under the situation of large k^*, the thermophoretic mobility of the particle first goes

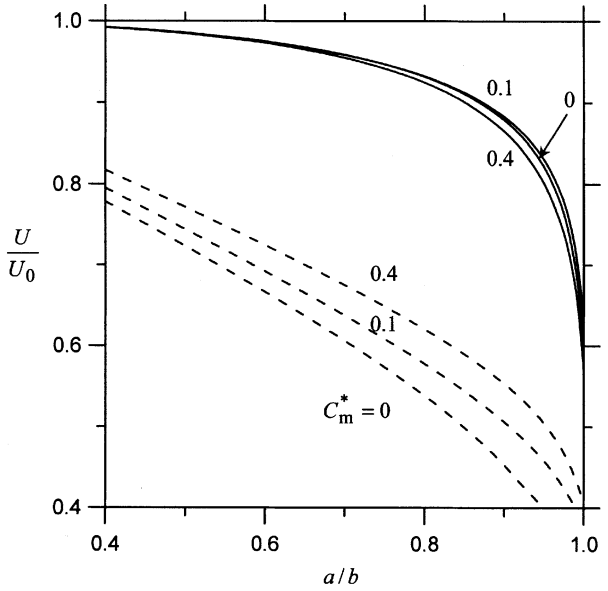

Figure 5. Normalized thermophoretic mobility [solid curves, with $C_t^* = 2C_m$ and $k^* = (1 - C_t^*)^{-1}$] and sedimenting mobility (dashed curves) of a spherical particle migrating parallel to a plane wall vs. separation parameter *a/b* for different values of C_m^*.

Table 3. Normalized Thermophoretic Velocity of a Spherical Particle along the Median Plane between Two Parallel Plane Walls with $C_t^* = C_m^* = 0$*

	U/U_0			
	$k^* = 0$		$k^* = 10$	
a/b	Exact Solution	Asymptotic Solution	Exact Solution	Asymptotic Solution
	For insulated plane walls			
0.2	0.99796	0.99796	0.99497	0.99497
0.4	0.98597	0.98617	0.96241	0.96288
0.6	0.96339	0.96661	0.88479	0.89411
0.8	0.94684	0.96326	0.74853	0.81948
0.9	0.96662	0.98325	0.64244	0.80784
0.95	1.0163	1.00270	0.5649	0.81679
0.99	1.2243	1.02412	0.4577	0.83402
0.995	1.362		0.441	
0.999	1.712		0.446	
	For plane walls prescribed with the far-field temperature profile			
0.2	0.99586	0.99587	0.99811	0.99811
0.4	0.96931	0.96975	0.98717	0.98736
0.6	0.90602	0.91448	0.96745	0.97058
0.8	0.79069	0.85485	0.95706	0.97239
0.9	0.69390	0.84471	0.98248	0.99596
0.95	0.6184	0.85078	1.0352	1.01744
0.99	0.5075	0.86316	1.2164	1.04060
0.995	0.490		1.324	
0.999	0.495		1.582	

*Computed from the Exact Boundary–Collocation Solution and the Asymptotic Method-of-Reflection Solution.

through a minimum with the increase of a/b from $a/b = 0$ and then increases monotonically, and the particle can even move faster than it would be at $a/b = 0$. This result indicates that the effect of thermal enhancement, rather than that of hydrodynamic resistance, can be overriding when the particle-wall gap thickness is small. An examination of the asymptotic formula for U/U_0 in Eq. A20 also shows a good agreement of the trend in Figure 6 with the analytical solution.

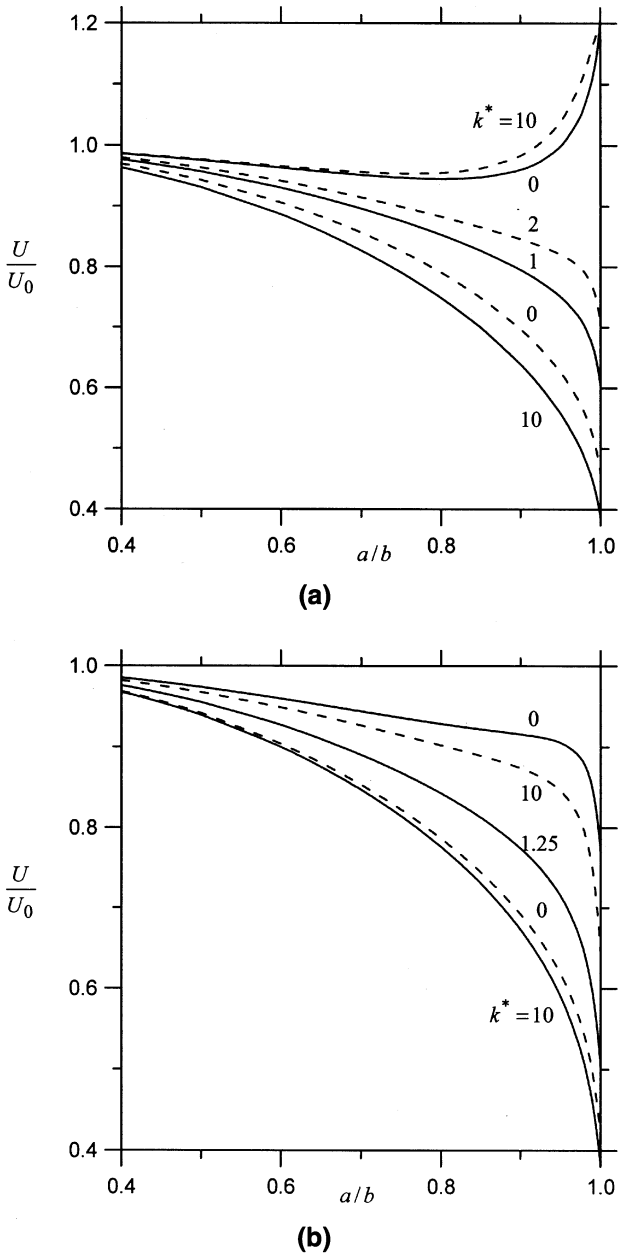

Figure 6. Normalized thermophoretic mobility U/U_0 of a spherical particle migrating on the median plane between two parallel plane walls (with $c = b$) vs. separation parameter a/b for several values of k^*.

(a) $C_t^* = 2C_m^* = 0.02$; (b) $C_t^* = 2C_m^* = 0.2$. The solid curves represent the case of insulated walls, and the dashed curves denote the case of walls prescribed with the far-field temperature distribution.

A careful comparison of the curves in Figure 6a for the case of a slit with the corresponding curves in Figure 2a for the case of a single wall reveals an interesting feature of the boundary effect on thermophoresis of an aerosol sphere. The presence of a second, identical, lateral plane wall, even at a symmetric position with respect to the sphere against the first, does not always enhance the wall effect on the thermophoretic particle induced by the first plate only. This result reflects again the fact that the lateral wall can affect the thermal driving force and the viscous drag force on a particle in opposite directions. Each force is increased in its own direction as the value of a/b turns small, but to a different degree, for the case of thermophoretic motion of a particle in a slit relative to that for the case of migration parallel to a single plate. Thus, the net effect composed of these two opposite forces for the slit case is not necessarily to enhance that for the case of a single wall.

Figure 7 shows the collocation results for the normalized translational velocity U/U_0 and rotational velocity $a\Omega/U_0$ of an aerosol sphere undergoing thermophoresis parallel to two plane walls at various positions between them for the case with $k^* = (1 - C_t^*)^{-1}$ and $C_t^* = 2C_m^* = 0.2$. The dashed curves (with $a/b =$ constant) illustrate the effect of the position of the second wall (at $z = c$) on the particle velocities for various values of the relative sphere-to-first-wall spacing b/a. The solid curves [with $2a/(b + c) =$ constant] indicate the variation of the particle velocities as functions of the sphere position at various values of the relative wall-to-wall spacing $(b + c)/2a$. As illustrated in Figure 7a, the net wall effect for the given case is to reduce the thermophoretic mobility U/U_0 of the particle. At a constant value of $2a/(b + c)$, the particle experiences a minimum viscous drag force and has the greatest translational velocity (without rotation) when it is located midway between the two walls (with $c = b$). The hydrodynamic drag increases, the translational velocity decreases, and the rotational velocity increases as the particle approaches either of the walls (or the ratio $b/(b + c)$ decreases).

At a specified value of a/b for the thermophoretic particle near a first lateral wall, the presence of a second plate is to further reduce the translational and rotational velocities of the particle, and the degree of this reduction increases monotonically with a decrease in the relative distance between the particle and the second plate (or with an increase in $b/(b + c)$).

On the other hand, for some cases such as the migration of an aerosol sphere with a small value of k^* parallel to two insulated plane walls or with a large value of k^* parallel to two plates prescribed with the far-field temperature distribution, as shown in Figure 8 for the latter case ($k^* = 100$), the net wall effect can increase the thermophoretic mobility of the particle relative to its isolated value (when the values of C_t^* and C_m^* are small). At a fixed value of $2a/(b + c)$ in these cases, the normalized thermophoretic mobility of the particle has a relatively small value, as it is located midway between the two walls, where the particle experiences a minimum effect of thermal enhancement, and becomes relatively large when it approaches either of the walls (this dependence is not graphically presented here for conciseness). At a given value of a/b for the thermophoretic particle and the first lateral plate, the effect induced by the presence of the sec-

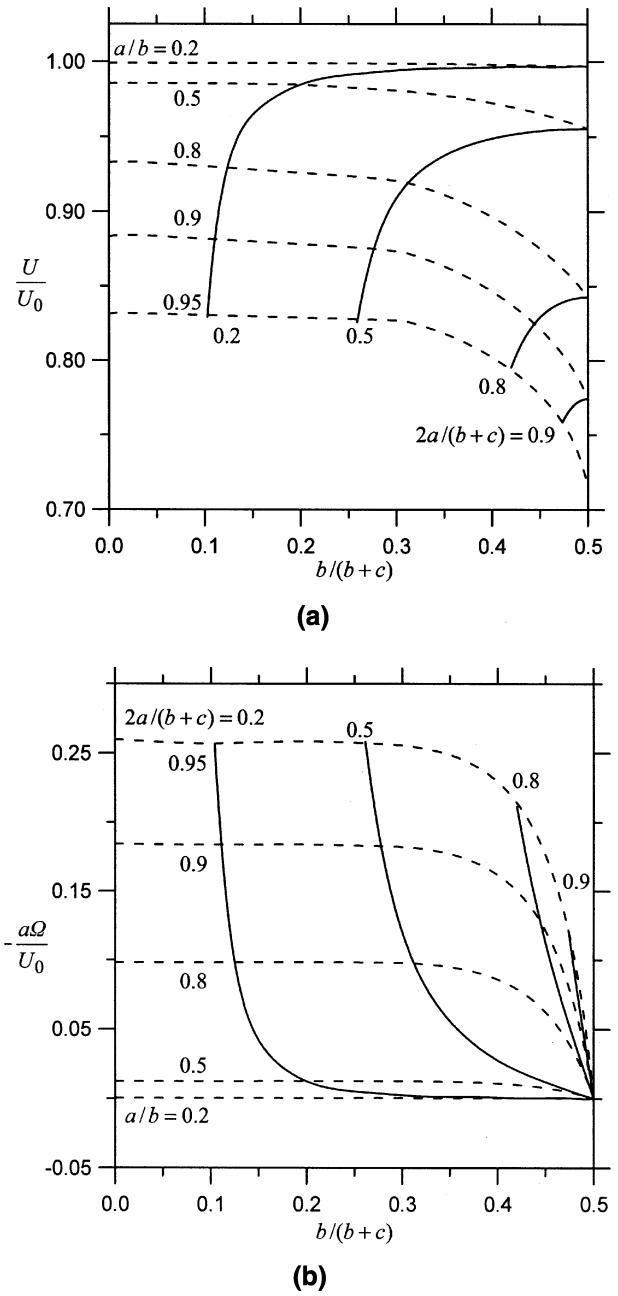

Figure 7. Normalized velocities of a spherical particle undergoing thermophoresis parallel to two plane walls vs. ratio $b/(b+c)$ for $C_t^* = 2C_m^* = 0.2$ and $k^* = (1 - C_t^*)^{-1}$ with a/b and $2a/(b+c)$ as parameters.

(a) Translational velocity U/U_0; (b) rotational velocity $a\Omega/U_0$.

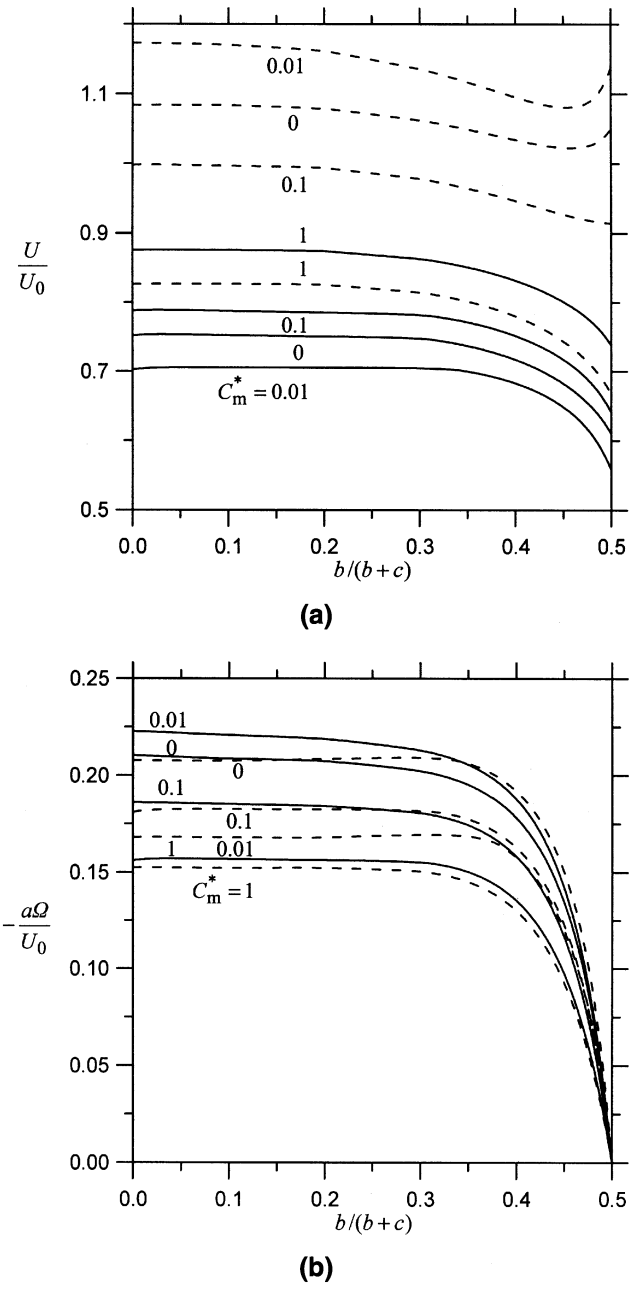

Figure 8. Normalized velocities of a spherical particle undergoing thermophoresis parallel to two plane walls vs. ratio $b/(b+c)$ for the case of $C_t^* = 2C_m^*$, $k^* = 100$, and $a/b = 0.9$ with C_t^* as a parameter.

(a) Translational velocity U/U_0; (b) rotational velocity $a\Omega/U_0$. The solid curves represent the case of insulated walls, and the dashed curves denote the case of walls prescribed with the far-field temperature distribution.

ond plate on the particle mobility is not necessarily a monotonic function of its distance from the particle. Again, the effect of variation in C_t^* $(= 2C_m^*)$ on the wall-corrected normalized particle velocities U/U_0 and $a\Omega/U_0$ does not exhibit a monotonic trend.

The collocation solution for the problem of sedimentation of an aerosol sphere with a slip-flow surface parallel to two plane walls at an arbitrary position between them was also obtained (Chen and Keh, 2003). Comparing that solution with the present results, we still find that the wall effect on thermophoresis in general is much weaker than that on sedimentation.

Conclusions

In this work, the exact numerical solutions and approximate analytical solutions for the steady thermophoretic motion of an aerosol sphere parallel to two infinite plane walls at an arbitrary position between them have been obtained by using the boundary–collocation technique and the method of reflections, respectively. Both the cases of insulated walls and of walls with the imposed far-field temperature gradient were examined in the limit of vanishingly small Reynolds and Peclet numbers. It has been found that the boundary effect on the thermophoretic motion of a particle is quite complicated. The thermophoretic mobility of a particle near a wall is generally, but not necessarily, a monotonic decreasing function of the separation parameter, a/b. When the value of a/b is close to unity, the effect of a lateral wall can speed up or slow down the particle velocity relative to its isolated value depending on the value of the parameter k^* of the particle and the thermal boundary condition at the wall. This behavior reflects the competition between the weak hydrodynamic retardation exerted by the neighboring wall on the particle migration and the possible, relatively strong thermophoretic enhancement due to the thermal interaction between the particle and the lateral wall.

Acknowledgment

This research was partly supported by the National Science Council of the Republic of China.

Notation

a = radius of the particle, m
A = thermophoretic mobility defined by Eq. 3, $m^2 \cdot s^{-1} \cdot K^{-1}$
A_n, B_n, C_n = coefficients in Eq. 20 for the flow field, $m^{n+1} \cdot s^{-1}$, $m^{n+3} \cdot s^{-1}$, $m^{n+2} \cdot s^{-1}$
B = coefficient defined right after Eq. A8, $m^2 \cdot s^{-1} \cdot K^{-1}$
b, c = the respective distances from the particle center to the two plates, m
C_1, C_2 = dimensionless parameters defined right after Eq. A8
C_m = dimensionless coefficient accounting for the frictional slip
$C_m^* = C_m l/a$
C_s = dimensionless coefficient accounting for the thermal slip
C_t = dimensionless coefficient accounting for the temperature jump
$C_t^* = C_t l/a$
D = dimensionless parameter defined right after Eq. A3
$\boldsymbol{e}_x, \boldsymbol{e}_y, \boldsymbol{e}_z$ = unit vectors in rectangular coordinates
$\boldsymbol{e}_r, \boldsymbol{e}_\theta, \boldsymbol{e}_\phi$ = unit vectors in spherical coordinates
$E_\infty = |\nabla T_\infty|$, $K \cdot m^{-1}$
G = dimensionless parameter defined right after Eq. A4
k = thermal conductivity of the fluid, $W \cdot m^{-1} \cdot K^{-1}$
k_1 = thermal conductivity of the particle, $W \cdot m^{-1} \cdot K^{-1}$
$k^* = k_1/k$
l = mean free path of the gas molecules, m
P_n^1 = the associated Legendre function of order n and degree one
r = radial spherical coordinate, m
R_n = coefficients in Eqs. 11 and 13 for the temperature field T, m^{n+2}
$\overline{R}_n$ = coefficients in Eq. 12 for the temperature field T_1, m^{-n+1}
T = temperature field in the fluid, K
T_1 = temperature field inside the particle, K
T_0 = mean gas temperature in the vicinity of the particle, K
T_∞ = prescribed temperature field defined by Eq. 7, K
$\boldsymbol{U}, U$ = translational velocity of the particle, $m \cdot s^{-1}$
$\boldsymbol{U}_0, U_0$ = thermophoretic velocity of an isolated particle defined by Eq. 1, $m \cdot s^{-1}$
$\boldsymbol{v}$ = velocity field of the fluid, $m \cdot s^{-1}$
x, y, z = rectangular coordinates, m

Greek letters

$\delta_n^{(1)}, \delta_n^{(2)}, \delta_n^{(3)}$ = functions of r and μ defined by Eqs. B1–B3, m^{-n-1}, m^{-n-2}, m^{-n-1}
η = viscosity of the fluid, $kg \cdot m^{-1} \cdot s^{-1}$
θ, ϕ = angular spherical coordinates
$\lambda = a/b$
$\mu = \cos\theta$
ρ = radial cylindrical coordinate, m
ρ_f = density of the fluid, $kg \cdot m^{-3}$
$\boldsymbol{\Omega}, \Omega$ = angular velocity of the particle, s^{-1}

Subscripts and superscripts

p = particle
w = wall
(i) = the ith reflection

Literature Cited

Bakanov, S. P., "Thermophoresis in Gases at Small Knudsen Numbers," *Aerosol Sci. Technol.*, **15**, 77 (1991).

Batchelor, G. K., and C. Shen, "Thermophoretic Deposition of Particles in Gas Flowing Over Cold Surfaces," *J. Colloid Interface Sci.*, **107**, 21 (1985).

Brock, J. R., "On the Theory of Thermal Forces Acting on Aerosol Particles," *J. Colloid Sci.*, **17**, 768 (1962).

Chen, P. Y., and H. J. Keh, "Slow Motion of a Slip Spherical Particle Parallel to One or Two Plane Walls," *J. Chin. Inst. Chem. Eng.*, **34**, 123 (2003).

Chen, S. H., "Boundary Effects on a Thermophoretic Sphere in an Arbitrary Direction of a Plane Surface," *AIChE J.*, **46**, 2352 (2000).

Chen, S. H., and H. J. Keh, "Axisymmetric Thermophoretic Motion of Two Spheres," *J. Aerosol Sci.*, **26**, 429 (1995).

Friedlander, S. K., *Smoke, Dust and Haze*, Wiley, New York (1977).

Ganatos, P., S. Weinbaum, and R. Pfeffer, "A Strong Interaction Theory for the Creeping Motion of a Sphere Between Plane Parallel Boundaries. Part 2. Parallel Motion," *J. Fluid Mech.*, **99**, 755 (1980).

Happel, J., and H. Brenner, *Low Reynolds Number Hydrodynamics*, Nijhoff, Dordrecht, The Netherlands (1983).

Keh, H. J., and J. H. Chang, "Boundary Effects on the Creeping-Flow and Thermophoretic Motions of an Aerosol Particle in a Spherical Cavity," *Chem. Eng. Sci.*, **53**, 2365 (1998).

Keh, H. J., and S. B. Chen, "Electrophoresis of a Colloidal Sphere Parallel to a Dielectric Plane," *J. Fluid Mech.*, **194**, 377 (1988).

Keh, H. J., and S. H. Chen, "Particle Interactions in Thermophoresis," *Chem. Eng. Sci.*, **50**, 3395 (1995).

Kennard, E. H., *Kinetic Theory of Gases*, McGraw-Hill, New York (1938).

Li, W., and E. J. Davis, "Measurement of the Thermophoretic Force by Electrodynamic Levitation: Microspheres in Air," *J. Aerosol Sci.*, **26**, 1063 (1995).

Loyalka, S. K., "Thermophoretic Force on a Single Particle—I. Numerical Solution of the Lineralized Boltzmann Equation," *J. Aerosol Sci.*, **23**, 291 (1992).

Lu, S.-Y., and C.-T. Lee, "Thermophoretic Motion of an Aerosol Particle in a Non-Concentric Pore," *J. Aerosol Sci.*, **32**, 1341 (2001).

Montassier, N., D. Boulaud, and A. Renoux, "Experimental Study of Thermophoretic Particle Deposition in Laminar Tube Flow," *J. Aerosol Sci.*, **22**, 677 (1991).

Morse, T. F., C. Y. Wang, and J. W. Cipolla, "Laser-Induced Thermophoresis and Particle Deposition Efficiency," *J. Heat Transfer*, **107**, 155 (1985).

O'Brien, V., "Form Factors for Deformed Spheroids in Stokes Flow," *AIChE J.*, **14**, 870 (1968).

O'Neill, M. E., "A Slow Motion of Viscous Liquid Caused by a Slowly Moving Solid Sphere," *Mathematika*, **11**, 67 (1964).

Sasse, A. G. B. M., W. W. Nazaroff, and A. J. Gadgil, "Particle Filter Based on Thermophoretic Deposition from Nature Convection Flow," *Aerosol Sci. Technol.*, **20**, 227 (1994).
Simpkins, P. G., S. Greenberg-Kosinski, and J. B. MacChesney, "Thermophoresis: The Mass Transfer Mechanism in Modified Chemical Vapor Deposition," *J. Appl. Phys.*, **50**, 5676 (1979).
Talbot, L., R. K. Cheng, R. W. Schefer, and D. R. Willis, "Thermophoresis of Particles in Heated Boundary Layer," *J. Fluid Mech.*, **101**, 737 (1980).
Waldmann, L., and K. H. Schmitt, "Thermophoresis and Diffusiophoresis of Aerosols," *Aerosol Science*, C. N. Davies, ed., Academic Press, New York (1966).
Weinberg, M. C., "Thermophoretic Efficiency in Modified Chemical Vapor Deposition Process," *J. Amer. Ceram. Soc.*, **65**, 81 (1982).
Whitmore, P. J., "Thermo- and Diffusiophoresis for Small Aerosol Particles," *J. Aerosol Sci.*, **12**, 1 (1981).
Williams, M. M. R., "Thermophoretic Forces Acting on a Spheroid," *J. Phys. D.*, **19**, 1631 (1986).
Williams, M. M. R., and S. K. Loyalka, *Aerosol Science: Theory and Practice, with Special Applications to the Nuclear Industry*, Pergamon Press, Oxford (1991).
Ye, Y., D. Y. H. Pui, B. Y. H. Liu, S. Opiolka, S. Blumhorst, and H. Fissan, "Thermophoretic Effect of Particle Deposition on a Free Standing Semiconductor Wafer in a Clean Room," *J. Aerosol Sci.*, **22**, 63 (1991).

Appendix A: Analysis of the Thermophoresis of Spherical Particle Parallel to Plane Walls by Method of Reflections

In this Appendix, we analyze the steady thermophoretic motion of an aerosol sphere with the relative thermal conductivity, k^*, temperature jump coefficient, C_t^*, and frictional slip coefficient, C_m^*, either parallel to an infinite flat wall ($c \to \infty$) or on the median plane between two parallel plates ($c = b$), as shown in Figure 1, by the method of reflections. The effect of the walls on the translational velocity $\boldsymbol{U}$ and angular velocity $\boldsymbol{\Omega}$ of the particle is sought in expansions of λ, which equals a/b, the ratio of the particle radius to the distance between the wall and the center of the particle.

Motion parallel to an infinite plane wall

For the problem of thermophoretic motion of a spherical particle parallel to an insulated plane wall, the governing equations (Eqs. 4 and 15) must be solved by satisfying the boundary conditions 5–7 and 16–18 with $c \to \infty$. The method-of-reflection solution consists of the following series, whose terms depend on increasing powers of λ

$$T = T_0 - E_\infty x + T_p^{(1)} + T_w^{(1)} + T_p^{(2)} + T_w^{(2)} + \cdots \quad \text{(A1a)}$$

$$\boldsymbol{v} = \boldsymbol{v}_p^{(1)} + \boldsymbol{v}_w^{(1)} + \boldsymbol{v}_p^{(2)} + \boldsymbol{v}_w^{(2)} + \cdots \quad \text{(A1b)}$$

where subscripts w and p represent the reflections from wall and particle, respectively, and the superscript (i) denotes the ith reflection from that surface. In these series, all the expansion sets of the corresponding temperature and velocity for the fluid phase must satisfy Eqs. 4a and 15. The advantage of this method is that it is necessary to consider boundary conditions associated with only one surface at a time.

According to Eq. A1, the translational and angular velocities of the particle can also be expressed in the series form

$$\boldsymbol{U} = U_0 \boldsymbol{e}_x + \boldsymbol{U}^{(1)} + \boldsymbol{U}^{(2)} + \cdots \quad \text{(A2a)}$$

$$\boldsymbol{\Omega} = \boldsymbol{\Omega}^{(1)} + \boldsymbol{\Omega}^{(2)} + \cdots \quad \text{(A2b)}$$

In these expressions, $U_0 = AE_\infty$ is the thermophoretic velocity of an identical particle suspended freely in the continuous phase far from the wall given by Eqs. 1 and 3; $\boldsymbol{U}^{(i)}$ and $\boldsymbol{\Omega}^{(i)}$ are related to $\nabla T_w^{(i)}$ and $\boldsymbol{v}_w^{(i)}$ by (Keh and Chen, 1995)

$$\boldsymbol{U}^{(i)} = -A\left[\nabla T_w^{(i)}\right]_0 + \left[\boldsymbol{v}_w^{(i)}\right]_0 + \frac{a^2 D}{6}\left[\nabla^2 \boldsymbol{v}_w^{(i)}\right]_0 \quad \text{(A3a)}$$

$$\boldsymbol{\Omega}^{(i)} = \frac{1}{2}\left[\nabla \times \boldsymbol{v}_w^{(i)}\right]_0 \quad \text{(A3b)}$$

Here, $D = (1 + 2C_m^*)^{-1}$ and the subscript 0 to variables inside brackets denotes evaluation at the position of the particle center.

The solution for the first reflected fields from the particle is

$$T_p^{(1)} = -GE_\infty a^3 r^{-2} \sin\theta \cos\phi \quad \text{(A4a)}$$

$$\boldsymbol{v}_p^{(1)} = \frac{1}{2} U_0 a^3 r^{-3}\left(2\sin\theta\cos\phi\,\boldsymbol{e}_r - \cos\theta\cos\phi\,\boldsymbol{e}_\theta + \sin\phi\,\boldsymbol{e}_\phi\right) \quad \text{(A4b)}$$

where $G = (1 - k^* + k^* C_t^*)(2 + k^* + 2k^* C_t^*)^{-1}$. Obviously, $-1 \le G \le 1/2$, with the upper and lower bounds occurring at the limits $k^* = 0$ and $k^* \to \infty$ (when $C_t^* \ll 1$), respectively. The velocity distribution shown in Eq. A4b is identical to the irrotational flow surrounding a rigid sphere moving with velocity $U_0 \boldsymbol{e}_x$.

The boundary conditions for the ith reflected fields from the wall are derived from Eqs. 6, 7, 17, and 18,

$$z = -b: \quad \frac{\partial T_w^{(i)}}{\partial z} = -\frac{\partial T_p^{(i)}}{\partial z} \quad \text{(A5a)}$$

$$\boldsymbol{v}_w^{(i)} = -\boldsymbol{v}_p^{(i)} \quad \text{(A5b)}$$

$$r \to \infty,\ z > -b: \quad T_w^{(i)} \to 0 \quad \text{(A5c)}$$

$$\boldsymbol{v}_w^{(i)} \to \boldsymbol{0} \quad \text{(A5d)}$$

The solution of $T_w^{(1)}$ is obtained by applying complex Fourier transforms on x and y in Eqs. 4a, A5a, and A5c (taking $i = 1$), with the result

$$T_w^{(1)} = -GE_\infty a^3 x\left[x^2 + y^2 + (z + 2b)^2\right]^{-3/2} \quad \text{(A6a)}$$

This reflected temperature field can be interpreted as arising from the reflection of the imposed field $-E_\infty \boldsymbol{e}_x$ from a fictitious particle identical to the actual particle, its location being at the mirror-image position of the actual particle with respect to the plane $z = -b$ (that is, at $x = 0$, $y = 0$, $z = -2b$). The solution for $\boldsymbol{v}_w^{(1)}$ can be found by fitting the

boundary conditions Eqs. A5b and A5d with the general solution to Eq. 15 established by Faxen (Happel and Brenner, 1983, p. 323), which results in

$$\boldsymbol{v}_w^{(1)} = \frac{U_0 a^3}{4\pi}\int_{-\infty}^{\infty}\int_{-\infty}^{\infty} e^{i(\alpha x+\beta y)-\kappa(z+2b)} \times\Big\{-\big[2\kappa(z+b)+1\big] i\alpha \boldsymbol{e}_z - \big[2\kappa(z+b)-1\big]\left(\frac{\alpha^2}{\kappa}\boldsymbol{e}_x+\frac{\alpha\beta}{\kappa}\boldsymbol{e}_y\right)\Big\} d\alpha d\beta \quad \text{(A6b)}$$

where $\kappa=(\alpha^2+\beta^2)^{1/2}$ and $i=\sqrt{-1}$.

The contributions of $T_w^{(1)}$ and $\boldsymbol{v}_w^{(1)}$ to the translational and angular velocities of the particle are determined by using Eq. A3

$$\boldsymbol{U}_t^{(1)} = -A\left[\nabla T_w^{(1)}\right]_{r=0} = \frac{1}{8}G\lambda^3 U_0 \boldsymbol{e}_x \quad \text{(A7a)}$$

$$\boldsymbol{U}_h^{(1)} = \left[\boldsymbol{v}_w^{(1)} + \frac{a^2 D}{6}\nabla^2 \boldsymbol{v}_w^{(1)}\right]_{r=0} = -\frac{1}{8}(\lambda^3 - D\lambda^5)U_0\boldsymbol{e}_x \quad \text{(A7b)}$$

$$\boldsymbol{U}^{(1)} = \boldsymbol{U}_t^{(1)} + \boldsymbol{U}_h^{(1)} = \frac{1}{8}\left[-(1-G)\lambda^3 + D\lambda^5\right]U_0\boldsymbol{e}_x \quad \text{(A7c)}$$

$$a\boldsymbol{\Omega}^{(1)} = \frac{a}{2}\left[\nabla\times\boldsymbol{v}_w^{(1)}\right]_{r=0} = -\frac{3}{16}\lambda^4 U_0\boldsymbol{e}_y \quad \text{(A7d)}$$

Equation A7a shows that the reflected temperature field from the insulated wall can increase (if $G>0$ or $k^*<(1-C_t^*)^{-1}$) or decrease (if $G<0$ or $k^*>(1-C_t^*)^{-1}$) the translational velocity of the thermophoretic particle, while Eq. A7b indicates that the reflected velocity field is to decrease this velocity; the net effect of the reflected fields is expressed by Eq. A7c, which can enhance or retard the movement of the particle, depending on the combination of the values of G (or k^* and C_t^*), D (or C_m^*), and λ. When $G=0$ (or $k^*=(1-C_t^*)^{-1}$), the reflected temperature field makes no contribution to the thermophoretic velocity. Equation A7c indicates that the wall correction to the translational velocity of the thermophoretic particle is $O(\lambda^3)$, which is weaker than that obtained for the corresponding sedimentation problem, in which the leading boundary effect is $O(\lambda)$. Note that, when the values of C_t^* and C_m^* are small, the necessary condition for the wall enhancement on the thermophoretic motion to occur is a small value of k^* and a value of λ close to unity such that the relation $D\lambda^5>(1-G)\lambda^3$ is warranted.

Equation A7d shows that the thermophoretic sphere rotates about an axis that is perpendicular to the direction of the applied gradient and parallel to the plane wall. The direction of rotation is opposite to that which would occur if the sphere were driven to move by a body force. Note that the angular velocity $\boldsymbol{\Omega}^{(1)}$ in Eq. A7d does not depend on the parameters G and D (since $\boldsymbol{v}_w^{(1)}$ is not a function of G and D). Also, the wall-induced angular velocity of the thermophoretic particle is $O(\lambda^4)$, which is the same in order as, but different, in its coefficient ($-3/16$ vs. $3/32$) from that of a rigid sphere moving under a body force field (Happel and Brenner, 1983, p. 327).

The solution for the second reflected fields from the particle is

$$T_p^{(2)} = -\frac{1}{8}E_\infty\big[G^2\lambda^3 a^3 r^{-2}\sin\theta\cos\phi + 3GH\lambda^4 a^4 r^{-3}\cos\theta\sin\theta\cos\phi + O(\lambda^5 a^5)\big] \quad \text{(A8a)}$$

$$\boldsymbol{v}_p^{(2)} = \frac{1}{32}U_0\big[2G\lambda^3 a^3 r^{-3}(2\sin\theta\cos\phi\boldsymbol{e}_r - \cos\theta\cos\phi\boldsymbol{e}_\theta + \sin\phi\boldsymbol{e}_\phi) + \left(48G\frac{B}{A}+60C_1\right)\lambda^4 a^2 r^{-2}\cos\theta\sin\theta\cos\phi\boldsymbol{e}_r + 3C_2\lambda^4 a^2 r^{-2}(\cos\phi\boldsymbol{e}_\theta - \cos\theta\sin\phi\boldsymbol{e}_\phi) + O(\lambda^4 a^4, \lambda^5 a^3)\big] \quad \text{(A8b)}$$

Here, $H=\alpha_1(1-k^*+2k^*C_t^*)$, $B=(5C_s\eta/2\rho_f T_0)\alpha_1\alpha_2(1+2k^*C_t^*)$, $C_1=\alpha_2(1+2C_m^*)$, and $C_2=(1+3C_m^*)^{-1}$, with $\alpha_1=(3+2k^*+6k^*C_t^*)^{-1}$ and $\alpha_2=(1+5C_m^*)^{-1}$.

The boundary conditions for the second reflected fields from the wall are obtained by substituting the results of $T_p^{(2)}$ and $\boldsymbol{v}_p^{(2)}$ into Eq. A5, with which Eqs. 4a and 15 can be solved as before to yield

$$\left[\nabla T_w^{(2)}\right]_{r=0} = -\left[\frac{1}{64}G^2\lambda^6 + O(\lambda^8)\right]E_\infty\boldsymbol{e}_x \quad \text{(A9a)}$$

$$\left[\boldsymbol{v}_w^{(2)}\right]_{r=0} = \left\{-\frac{1}{256}\left[4G\left(1+9\frac{B}{A}\right)-45C_1\right]\lambda^6 + O(\lambda^8)\right\}U_0\boldsymbol{e}_x \quad \text{(A9b)}$$

The contribution of the second reflected fields to the translational and angular velocities of the particle is obtained by combining Eqs. A3 and A9, which gives

$$\boldsymbol{U}^{(2)} = \left\{\frac{1}{256}\left[4G^2 - 4G\left(1+9\frac{B}{A}\right)-45C_1\right]\lambda^6 + O(\lambda^8)\right\}U_0\boldsymbol{e}_x \quad \text{(A10a)}$$

$$a\boldsymbol{\Omega}^{(2)} = \left[-\frac{1}{1{,}024}\left(18G+72\frac{B}{A}G+90C_1+15C_2\right)\lambda^7 + O(\lambda^9)\right]U_0\boldsymbol{e}_y \quad \text{(A10b)}$$

The errors for $\boldsymbol{U}^{(2)}$ and $a\boldsymbol{\Omega}^{(2)}$ are $O(\lambda^8)$ and $O(\lambda^9)$, respectively, because the $O(\lambda^7)$ terms in the expansions of $\nabla T_w^{(2)}$ and $\boldsymbol{v}_w^{(2)}$ vanish at the position of the particle center.

Obviously, $\boldsymbol{U}^{(3)}$ and $\alpha\boldsymbol{\Omega}^{(3)}$ will be $O(\lambda^9)$ and $O(\lambda^{10})$, respectively. With the substitution of Eqs. A7c, A7d, and A10

into Eq. A2, the particle velocities can be expressed as $\boldsymbol{U} = U\boldsymbol{e}_x$ and $\boldsymbol{\Omega} = \Omega \boldsymbol{e}_y$ with

$$U = U_0\left\{1 - \frac{1}{8}(1-G)\lambda^3 + \frac{D}{8}\lambda^5 + \frac{1}{256}\left[4G^2 - 4\left(1 + 9\frac{B}{A}\right)G - 45C_1\right]\lambda^6 + O(\lambda^8)\right\} \quad \text{(A11a)}$$

$$a\Omega = U_0\left[-\frac{3}{16}\lambda^4 - \frac{1}{1024}\left(18G + 72\frac{B}{A}G + 90C_1 + 15C_2\right) \times \lambda^7 + O(\lambda^9)\right] \quad \text{(A11b)}$$

The particle migrates along the imposed temperature gradient at a rate that can increase or decrease as the particle approaches the wall. Owing to the neglect of inertial effects, the wall does not deflect the direction of thermophoresis.

For the case that a linear temperature profile is prescribed on the plane wall that is consistent with the far-field distribution, namely, the boundary condition Eq. 6 is replaced by Eq. 8, the series expansions (Eqs. A1 and A2), the solution of $T_p^{(1)}$ and $\boldsymbol{v}_p^{(1)}$ in Eq. A4, and the boundary conditions for $T_w^{(i)}$ and $\boldsymbol{v}_w^{(i)}$ in Eqs. A5b–A5d are still valid, while Eq. A5a becomes

$$z = -b: \quad T_w^{(i)} = -T_p^{(i)} \quad \text{(A12)}$$

With this change, it can be shown that the results of the following reflected fields and of the particle velocities are also obtained from Eqs. A6–A11 by replacing G with $-G$. Thus, contrary to the effect of an insulated plane wall, the reflected temperature field from a parallel wall with the imposed far-field temperature gradient reduces the translational velocity of the particle if $G > 0$ or $k^* < (1 - C_t^*)^{-1}$ and enhances this velocity if $G < 0$ or $k^* > (1 - C_t^*)^{-1}$. When $G = 0$ or $k^* = (1 - C_t^*)^{-1}$, the two types of plane wall will produce the same effects (with no contribution from the reflected temperature field) on the thermophoretic motion of the particle. Under the condition that the values of C_t^* and C_m^* are small and the values of k^* and λ are sufficiently large such that $D\lambda^5 > (1 + G)\lambda^3$, the net effect of a lateral plane wall prescribed with the far-field temperature distribution can enhance the thermophoretic migration of a particle.

Motion on the median plane between two parallel flat walls

For the problem of thermophoretic motion of a sphere on the median plane between two insulated parallel plates, the boundary conditions corresponding to governing Eqs. 4a and 15 are given by Eqs. 5–7 and 16–18 with $c = b$. But, the angular velocity $\boldsymbol{\Omega}$ of the particle vanishes now because of the symmetry. With $\lambda = a/b \ll 1$, the series expansions of the temperature, fluid velocity, and particle velocity given by Eqs. A1, A2a, and A4 remain valid here. From Eqs. 6, 7, 17, and 18, the boundary conditions for $T_w^{(i)}$ and $\boldsymbol{v}_w^{(i)}$ are found to be

$$|z| = b: \quad \frac{\partial T_w^{(i)}}{\partial z} = -\frac{\partial T_p^{(i)}}{\partial z} \quad \text{(A13a)}$$

$$\boldsymbol{v}_w^{(i)} = -\boldsymbol{v}_p^{(i)} \quad \text{(A13b)}$$

$$r \to \infty, |z| \le b \quad T_w^{(i)} \to 0 \quad \text{(A13c)}$$

$$\boldsymbol{v}_w^{(i)} \to \boldsymbol{0} \quad \text{(A13d)}$$

The first wall-reflected fields can be solved by the same method as used for a single lateral plate in the previous subsection, with the results

$$T_w^{(1)} = \frac{GE_\infty a^3}{2\pi}\int_{-\infty}^{\infty}\int_{-\infty}^{\infty}\frac{i\alpha}{\kappa}e^{i(\alpha x + \beta y) - \kappa b}\frac{\cosh(\kappa z)}{\sinh(\kappa b)}d\alpha d\beta \quad \text{(A14a)}$$

$$\boldsymbol{v}_w^{(1)} = \frac{U_0 a^3}{2\pi}\int_{-\infty}^{\infty}\int_{-\infty}^{\infty}\frac{1}{\sinh(2\kappa b) - 2\kappa b}e^{i(\alpha x + \beta y)} \times \{[-\kappa z\cosh(\kappa z) + (1+g)\sinh(\kappa z)]i\alpha \boldsymbol{e}_z + [\kappa z\sinh(\kappa z) - g\cosh(\kappa z)]\left(\frac{\alpha^2}{\kappa}\boldsymbol{e}_x + \frac{\alpha\beta}{\kappa}\boldsymbol{e}_y\right)\}d\alpha d\beta \quad \text{(A14b)}$$

where $\kappa = (\alpha^2 + \beta^2)^{1/2}$ and $g = \kappa b - e^{-\kappa b}\sinh(\kappa b)$. The contributions of $T_w^{(1)}$ and $\boldsymbol{v}_w^{(1)}$ to the particle velocity are determined using Eq. A3a, which leads to a result similar to Eqs. A7a–A7c

$$\boldsymbol{U}_t^{(1)} = d_1 G\lambda^3 U_0 \boldsymbol{e}_x \quad \text{(A15a)}$$

$$\boldsymbol{U}_h^{(1)} = -\left(d_2\lambda^3 - d_3 D\lambda^5\right)U_0\boldsymbol{e}_x \quad \text{(A15b)}$$

$$\boldsymbol{U}^{(1)} = \boldsymbol{U}_t^{(1)} + \boldsymbol{U}_h^{(1)} = \left[-(d_2 - d_1 G)\lambda^3 + d_3 D\lambda^5\right]U_0\boldsymbol{e}_x \quad \text{(A15c)}$$

where

$$d_1 = \int_0^\infty \frac{\rho^2}{e^{2\rho} - 1}d\rho = 0.300514 \quad \text{(A16a)}$$

$$d_2 = \frac{1}{2}\int_0^\infty \frac{\rho^2(\rho - e^{-\rho}\sinh\rho)}{\sinh(2\rho) - 2\rho}d\rho = 0.417956 \quad \text{(A16b)}$$

$$d_3 = \frac{1}{6}\int_0^\infty \frac{\rho^4}{\sinh(2\rho) - 2\rho}d\rho = 0.338324 \quad \text{(A16c)}$$

Analogous to the previous case, the results of the second reflections can be obtained as

$$T_p^{(2)} = -E_\infty\left[d_1 G^2\lambda^3 a^3 r^{-2}\sin\theta\cos\phi + O(\lambda^5 a^5)\right] \quad \text{(A17a)}$$

$$\boldsymbol{v}_p^{(2)} = \frac{U_0}{2}\Big[d_1 G\lambda^3 a^3 r^{-3}\big(2\sin\theta\cos\phi\boldsymbol{e}_r - \cos\theta\cos\phi\boldsymbol{e}_\theta + \sin\phi\boldsymbol{e}_\phi\big) + O(\lambda^5 a^3)\Big] \quad \text{(A17b)}$$

$$\big[\nabla T_w^{(2)}\big]_{r=0} = -\big[d_1^2 G^2\lambda^6 + O(\lambda^8)\big]E_\infty \boldsymbol{e}_x \quad \text{(A18a)}$$

$$\big[\boldsymbol{v}_w^{(2)}\big]_{r=0} = \big[-d_1 d_2 G\lambda^6 + O(\lambda^8)\big]U_0\boldsymbol{e}_x \quad \text{(A18b)}$$

and

$$\boldsymbol{U}^{(2)} = \big[-\big(d_1 d_2 G - d_1^2 G^2\big)\lambda^6 + O(\lambda^8)\big]U_0\boldsymbol{e}_x \quad \text{(A19)}$$

Note that the $\lambda^4 a^2$ and $\lambda^4 a^4$ terms in the expressions for $T_p^{(2)}$ and $\boldsymbol{v}_p^{(2)}$ vanish. With the combination of Eqs. A2a, A15c, and A19, the particle velocity can be expressed as $\boldsymbol{U} = U\boldsymbol{e}_x$ with

$$U = U_0\big[1 - (d_2 - d_1 G)\lambda^3 + d_3 D\lambda^5 - \big(d_1 d_2 G - d_1^2 G^2\big)\lambda^6 + O(\lambda^8)\big] \quad \text{(A20)}$$

For the case that the particle is undergoing thermophoresis on the median plane between two parallel plates on which a linear temperature profile consistent with the far-field distribution is imposed, the boundary condition given by Eq. 6 should be replaced by Eq. 8. In this case, Eqs. A1, A2a, A4, and A13b–A13d are still applicable, while Eq. A13a becomes

$$|z| = b: \quad T_w^{(i)} = -T_p^{(i)} \quad \text{(A21)}$$

With this change, it can be shown that the results of the reflected fields and of the particle velocity are also obtained from Eqs. A14–A20 by replacing G and d_1 by $-G$ and $\bar{d}_1$, respectively, where

$$\bar{d}_1 = \int_0^\infty \frac{\rho^2}{e^{2\rho}+1}d\rho = 0.225386 \quad \text{(A22)}$$

Comparing Eq. A20 for the slit case with Eq. A11a for the case of a single parallel plane, one can find that the wall effects on the thermophoretic velocity of a particle in the two cases are qualitatively similar. However, the assumption that the result of the boundary effect for two walls can be obtained by simple addition of the single-wall effects generally gives a smaller correction to the thermophoretic velocity, while for the corresponding sedimentation problem this approximation overestimates the wall correction.

Appendix B: Definitions of Some Functions in the Second Section

The functions $\delta_n^{(i)}$ with $i = 1$, 2, and 3 in Eqs. 13, 14, and 21 are defined by

$$\delta_n^{(1)}(r,\mu) = r^{-n-1}P_n^1(\mu) - (-n)^m\int_0^\infty \kappa^{1-m}\frac{J_1(\kappa\rho)}{\sinh\tau}\times\Big[c^2 V_{n+m}(c)(\sinh\sigma)^{1-m}(\cosh\sigma)^m - b^2 V_{n+m}(-b)(\sinh\omega)^{1-m}(\cosh\omega)^m\Big]d\kappa \quad \text{(B1)}$$

$$\delta_n^{(2)}(r,\mu) = -(n+1)r^{-n-2}P_n^1(\mu) - (-n)^m\int_0^\infty \frac{\kappa^{2-m}}{\sinh\tau}\Big\{J_1'(\kappa\rho)(1-\mu^2)^{1/2}\times\Big[c^2 V_{n+m}(c)(\sinh\sigma)^{1-m}(\cosh\sigma)^m - b^2 V_{n+m}(-b)(\sinh\omega)^{1-m}(\cosh\omega)^m\Big] + J_1(\kappa\rho)\mu\Big[c^2 V_{n+m}(c)(\cosh\sigma)^{1-m}(\sinh\sigma)^m - b^2 V_{n+m}(-b)(\cosh\omega)^{1-m}(\sinh\omega)^m\Big]\Big\}d\kappa \quad \text{(B2)}$$

$$\delta_n^{(3)}(r,\mu) = -r^{-n-1}\frac{\partial P_n^1(\mu)}{\partial\mu}(1-\mu^2)^{1/2} - (-n)^m r\int_0^\infty \frac{\kappa^{2-m}}{\sinh\tau}\Big\{J_1'(\kappa\rho)\mu\times\Big[c^2 V_{n+m}(c)(\sinh\sigma)^{1-m}(\cosh\sigma)^m - b^2 V_{n+m}(-b)(\sinh\omega)^{1-m}(\cosh\omega)^m\Big] - J_1(\kappa\rho)(1-\mu^2)^{1/2}\Big[c^2 V_{n+m}(c)(\cosh\sigma)^{1-m}(\sinh\sigma)^m - b^2 V_{n+m}(-b)(\cosh\omega)^{1-m}(\sinh\omega)^m\Big]\Big\}d\kappa \quad \text{(B3)}$$

Here

$$V_n(z_i) = \frac{(2/\pi)^{1/2}}{z_i^{n+1}}\sum_{q=0}^{[n/2]}\frac{(\kappa|z_i|)^{n-q-(1/2)}}{(-2)^q q!(n-2q-1)!}\times K_{n-q-3/2}(\kappa|z_i|) \quad \text{(B4)}$$

$$\sigma = \kappa(z+b), \quad \omega = \kappa(z-c), \quad \tau = \kappa(b+c), \quad \text{(B5a,b,c)}$$

where J_1 is the Bessel function of the first kind of order one and the prime on it denotes differentiation with respect to its argument, K_υ is the modified Bessel function of the second kind of order υ, and the square bracket $[\upsilon]$ denotes the largest integer, which is less than or equal to υ. In Eqs. B1–B3, $m = 1$ if Eq. 6 is used for the boundary condition of the temperature field at the plane walls and $m = 0$ if Eq. 8 is used.

The starred A_n, B_n, and C_n functions in Eq. 21 are defined by

$$A_n^*(r,\mu,\phi) = (1-\mu^2)^{1/2}(A_n' + \alpha_n')\cos\phi + (1-\mu^2)^{1/2}(A_n'' + \alpha_n'')\sin\phi + \mu(A_n''' + \alpha_n''') \quad \text{(B6a)}$$

$$B_n^*(r,\mu,\phi) = (1-\mu^2)^{1/2}(B_n' + \beta_n')\cos\phi + (1-\mu^2)^{1/2}(B_n'' + \beta_n'')\sin\phi + \mu(B_n''' + \beta_n''') \quad \text{(B6b)}$$

$$C_n^*(r,\mu,\phi) = (1-\mu^2)^{1/2}(C_n' + \gamma_n')\cos\phi + (1-\mu^2)^{1/2}(C_n'' + \gamma_n'')\sin\phi + \mu(C_n''' + \gamma_n''') \quad \text{(B6c)}$$

$$A_n^{**}(r,\mu,\phi) = \mu(A_n' + \alpha_n')\cos\phi + \mu(A_n'' + \alpha_n'')\sin\phi - (1-\mu^2)^{1/2}(A_n''' + \alpha_n''') \quad \text{(B6d)}$$

$$B_n^{**}(r,\mu,\phi) = \mu(B_n' + \beta_n')\cos\phi + \mu(B_n'' + \beta_n'')\sin\phi - (1-\mu^2)^{1/2}(B_n''' + \beta_n''') \quad \text{(B6e)}$$

$$C_n^{**}(r,\mu,\phi) = \mu(C_n' + \gamma_n')\cos\phi + \mu(C_n'' + \gamma_n'')\sin\phi - (1-\mu^2)^{1/2}(C_n''' + \gamma_n''') \quad \text{(B6f)}$$

$$A_n^{***}(r,\mu,\phi) = -(A_n' + \alpha_n')\sin\phi + (A_n'' + \alpha_n'')\cos\phi \quad \text{(B6g)}$$

$$B_n^{***}(r,\mu,\phi) = -(B_n' + \beta_n')\sin\phi + (B_n'' + \beta_n'')\cos\phi \quad \text{(B6h)}$$

$$C_n^{***}(r,\mu,\phi) = -(C_n' + \gamma_n')\sin\phi + (C_n'' + \gamma_n'')\cos\phi \quad \text{(B6i)}$$

Here, the primed A_n, B_n, C_n, α_n, β_n, and γ_n are functions of the position in Eq. 20.

Manuscript received July 11, 2002, and revision received Feb. 24, 2003.